Title
Intravascular optical coherence tomography measurement of size and apposition of metallic stents.

Journal
Biomedical Optics Express, 4(10)

ISSN
2156-7085

Authors
Elahi, Sahar
Feldman, Marc
Dijkstra, Jouke
et al.

Publication Date
2013

DOI
10.1364/BOE.4.001876

Peer reviewed

Biomedical Optics EXPRESS

Intravascular optical coherence tomography measurement of size and apposition of metallic stents

Sahar Elahi,[1] Marc D. Feldman,[2] Jouke Dijkstra,[3] and Thomas E. Milner[1,*]

[1]*Department of Biomedical Engineering, University of Texas at Austin, USA*
[2]*Division of Cardiology, Department of Medicine, University of Texas Health Science Center at San Antonio, and the South Texas Veterans Affairs Health Care System, San Antonio, Texas, USA*
[3]*Department of Radiology, Leiden University Medical Center, the Netherlands*
**terra.laser@gmail.com*

Abstract: Effect of beam size and catheter position on the apparent size and apposition of metallic stent struts in IVOCT images were examined. Micro-CT data was employed to determine light - stent strut interactions. Simulated results suggest that location of the reflecting regions depend on relative orientation and position of stent struts to the IVOCT beam. Erroneous stent apposition measurements can occur when the IVOCT catheter is at an eccentric position. A method that mitigates stent strut apposition measurement errors is proposed.

OCIS codes: (110.0110) Imaging systems; (110.4500) Optical coherence tomography.

References and links

1. S. Mendis, P. Puska, and B. Norrving, "Global Atlas on Cardiovascular Disease Prevention and Control," WHO, Geneva (2011).
2. G. N. Levine, E. R. Bates, J. C. Blankenship, S. R. Bailey, J. A. Bittl, B. Cercek, C. E. Chambers, S. G. Ellis, R. A. Guyton, S. M. Hollenberg, U. N. Khot, R. A. Lange, L. Mauri, R. Mehran, I. D. Moussa, D. Mukherjee, B. K. Nallamothu, H. H. TingAmerican College of Cardiology FoundationAmerican Heart Association Task Force on Practice GuidelinesSociety for Cardiovascular Angiography and Interventions, "2011 ACCF/AHA/SCAI Guideline for Percutaneous Coronary Intervention. A Report of the American College of Cardiology Foundation/American Heart Association Task Force on Practice Guidelines and the Society for Cardiovascular Angiography and Interventions," J. Am. Coll. Cardiol. **58**(24), e44–e122 (2011).
3. M. E. Brezinski, G. J. Tearney, B. E. Bouma, J. A. Izatt, M. R. Hee, E. A. Swanson, J. F. Southern, and J. G. Fujimoto, "Optical Coherence Tomography for Optical Biopsy. Properties and Demonstration of Vascular Pathology," Circulation **93**(6), 1206–1213 (1996).
4. M. E. Brezinski, G. J. Tearney, N. J. Weissman, S. A. Boppart, B. E. Bouma, M. R. Hee, A. E. Weyman, E. A. Swanson, J. F. Southern, and J. G. Fujimoto, "Assessing atherosclerotic plaque morphology: comparison of optical coherence tomography and high frequency intravascular ultrasound," Heart **77**(5), 397–403 (1997).
5. J. G. Fujimoto, S. A. Boppart, G. J. Tearney, B. E. Bouma, C. Pitris, and M. E. Brezinski, "High resolution in vivo intra-arterial imaging with optical coherence tomography," Heart **82**(2), 128–133 (1999).
6. M. Brezinski, X. Li, H. Gold, N. Weissman, C. Pitris, K. Saunders, R. Ghanti, and J. Fujimoto, "In vivo intravascular imaging with OCT comparison with ultrasound," in *Conference on Biomedical Optical Spectroscopy and Diagnostics,* (Optical Society of America, 2000), paper SuC3.
7. J. W. Villard, K. K. Cheruku, and M. D. Feldman, "Applications of optical coherence tomography in cardiovascular medicine, part 1," J. Nucl. Cardiol. **16**(2), 287–303 (2009).
8. H. G. Bezerra, M. A. Costa, G. Guagliumi, A. M. Rollins, and D. I. Simon, "Intracoronary Optical Coherence Tomography: A Comprehensive Review," JACC Cardiovasc. Interv. **2**(11), 1035–1046 (2009).
9. G. J. Tearney, E. Regar, T. Akasaka, T. Adriaenssens, P. Barlis, H. G. Bezerra, B. Bouma, N. Bruining, J. M. Cho, S. Chowdhary, M. A. Costa, R. de Silva, J. Dijkstra, C. Di Mario, D. Dudek, E. Falk, M. D. Feldman, P. Fitzgerald, H. M. Garcia-Garcia, N. Gonzalo, J. F. Granada, G. Guagliumi, N. R. Holm, Y. Honda, F. Ikeno, M. Kawasaki, J. Kochman, L. Koltowski, T. Kubo, T. Kume, H. Kyono, C. C. S. Lam, G. Lamouche, D. P. Lee, M. B. Leon, A. Maehara, O. Manfrini, G. S. Mintz, K. Mizuno, M. A. Morel, S. Nadkarni, H. Okura, H. Otake, A. Pietrasik, F. Prati, L. Räber, M. D. Radu, J. Rieber, M. Riga, A. Rollins, M. Rosenberg, V. Sirbu, P. W. J. C. Serruys, K. Shimada, T. Shinke, J. Shite, E. Siegel, S. Sonoda, M. Suter, S. Takarada, A. Tanaka, M. Terashima, T. Thim, S. Uemura, G. J. Ughi, H. M. M. van Beusekom, A. F. W. van der Steen, G. A. van Es, G. van Soest, R. Virmani, S. Waxman, N. J. Weissman, and G. Weisz; International Working Group for Intravascular Optical

#189970 - $15.00 USD Received 6 May 2013; revised 24 Jul 2013; accepted 30 Jul 2013; published 30 Aug 2013

Coherence Tomography (IWG-IVOCT), "Consensus standards for acquisition, measurement, and reporting of intravascular optical coherence tomography studies: a report from the International working group for intravascular optical coherence tomography standardization and validation," J. Am. Coll. Cardiol. **59**(12), 1058–1072 (2012).
10. S. Elahi, J. J. Mancuso, T. E. Milner, and M. D. Feldman, "Sunflower Artifact in OCT," JACC Cardiovasc. Imaging **4**(11), 1220–1221 (2011).
11. S. Elahi, J. J. Mancuso, M. D. Feldman, J. Dijkstra, and T. E. Milner, "Effect of stent surface-scattering properties on IV-OCT images," Proc. SPIE **8207**, 820743 (2012).
12. M. Friebel, J. Helfmann, U. Netz, and M. Meinke, "Influence of oxygen saturation on the optical scattering properties of human red blood cells in the spectral range 250 to 2,000 nm," J. Biomed. Opt. **14**(3), 034001 (2009).
13. G. J. Ughi, T. Adriaenssens, K. Onsea, P. Kayaert, C. Dubois, P. Sinnaeve, M. Coosemans, W. Desmet, and J. D'hooge, "Automatic segmentation of in-vivo intra-coronary optical coherence tomography images to assess stent strut apposition and coverage," Int. J. Cardiovasc. Imaging **28**(2), 229–241 (2012).

1. Introduction

Coronary artery disease is the leading cause of death worldwide [1]. Coronary stent placement is a routine treatment option that reduces intraluminal vessel stenosis to restore normal myocardial blood flow both at rest and during exertion. Confirmation of complete stent apposition to the arterial wall immediately after deployment is important to reduce the incidence of late stent thrombosis [2]. Intravascular Optical Coherence Tomography (IVOCT) is a recently developed imaging modality with high axial resolution (5-15 μm) and sufficient tissue penetration depth of 1.5-2.0 mm to allow stent apposition assessment [3–7]. Although IVOCT does not penetrate tissue as deep as intravascular ultrasound (IVUS), finer image resolution of one order-of-magnitude allows IVOCT to provide stent apposition information that IVUS cannot offer and therefore gives IVOCT an important advantage.

Metallic stent struts typically appear as small bright line-segments in IVOCT images due to light reflection from the metal surface and do not represent the true stent strut surface profile. Vessel curvature and tortuosity can result in placement of the IVOCT catheter in an eccentric position in the lumen, giving rise to stent artifacts including the "sunflower effect", bending of stent struts toward the imaging catheter [8] and "merry-go-round" effect, variable apparent strut size. For instance, the size of a strut can appear smaller in IVOCT images acquired from an offset, Fig. 1(b), compared with a centered, Fig. 1(a), catheter position. Inasmuch as IVOCT stent measurements are at an early stage, no comprehensive consensus methodology exists on how to measure stent malapposition with off-center IVOCT catheter placement that is uniformly agreed upon [9]. In current IVOCT clinical practice, two approaches are utilized to measure stent malapposition: approach 1) the user draws a line-segment from center of the strut blooming in the IVOCT image to the luminal wall that indicates the shortest distance, Fig. 1(c), malapposition is determined by subtracting the known strut thickness from the measured distance; approach 2) a box representing the strut cross-section is positioned in the IVOCT image so that one box-edge is coincident with the leading edge of the IVOCT strut, blue box in Fig. 1(d), the user/software draws a line segment from the midpoint of the opposing box-edge to luminal wall that is perpendicular to the box-edge, length of this line indicates strut malapposition [8].

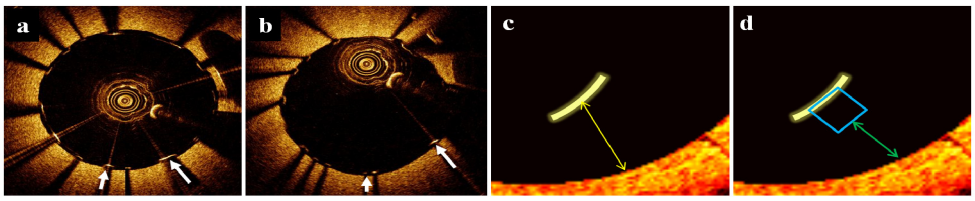

Fig. 1. Apparent strut size in a phantom: **a)** centered catheter, **b)** eccentric catheter where strut size minimized (both arrows) and sunflowered (large arrow), malapposition measurement: **c)** approach 1; yellow line is drawn from center of strut blooming to the luminal wall indicating the shortest distance, **d)** approach 2; box is positioned so that edge is coincident with the leading edge of the stent and green line is drawn perpendicular to the box-edge.

#189970 - $15.00 USD Received 6 May 2013; revised 24 Jul 2013; accepted 30 Jul 2013; published 30 Aug 2013

Recently Elahi et al. reported [10] studies involving coronary arteries, vessel phantoms and computer simulations that suggest light returning to an IVOCT catheter from a metallic strut surface reflects from a small and unspecified region with nearly constant optical pathlength. Elahi et al. suggested that additional studies using well-characterized stents may provide a better estimate of the location on the stent strut from where light is reflecting into the catheter. We present results of a study that models light reflection from an individual strut measured using Micro-CT to characterize three-dimensional IVOCT strut geometry. Using simulated IVOCT images, methods for correct box placement for various catheter-strut orientations are recommended so that artifacts are not introduced and stent apposition can be measured accurately.

2. Materials and methods

2.1. Micro-CT imaging

Vessel phantom construction and deployment of a 3 × 8 CYPHER® Sirolimus-eluting coronary stent (Cordis Corporation, Miami Lakes, Florida) were described previously [10,11]. High resolution Micro-CT imaging (Fig. 2) allowed simulation of light interaction between an IVOCT catheter and a single strut. A high resolution close-up scan of a CYPHER stent strut, Fig. 2(b) was acquired using an Xradia microXCT scanner giving 1024 images of 0.53 μm resolution (both in-plane and interslice). A three-dimensional representation of the strut was stored in a stereolithography (STL) file format, Fig. 2(c). Selected strut has a trapezoidal cross section with a 120 μm height, a 90 μm long edge, opposite the 130 μm long base facing the lumen.

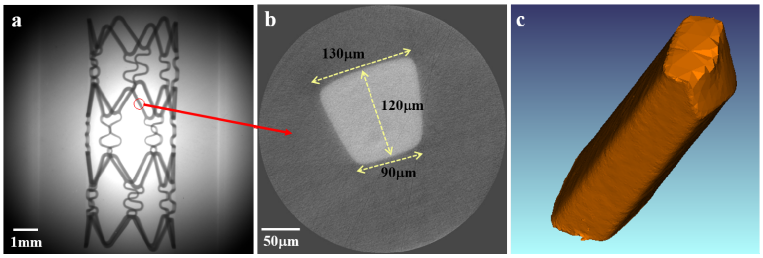

Fig. 2. **a)** Selected strut of a 3 × 8 CYPHER stent deployed in a 3mm diameter phantom vessel, **b)** cross sectional view of the strut, **c)** three dimensional STL of the stent strut comprised of 1024 cross sectional images (543microns).

2.2. Simulation of light-strut interaction

Simulation of light transmission in a 3.1 French IVOCT catheter including propagation and return of emitted light (1310 nm) was achieved using optical design software (ZEMAX, Radiant, Redmond, WA). Light from a single-mode optical fiber (SMF-28) with mode field diameter of 10 μm is focused by a GRIN lens (0.5 mm diameter, 1.32 mm length and peak refractive index of 1.629), reflects from a 0.150mm glass (BK7) 45° prism, propagates through saline (n = 1.34, 256 μm thick) to the polymer catheter sheath (r_o-r_i = 152 μm) and into the vessel lumen filled with a contrast flush with a numerical aperture of 0.14 (Fig. 3). The geometric beam size is 100 × 100 μm^2 at the prism and focuses to a minimum spot diameter along x- and y-axes at 1.13 mm and 1.21 mm from the catheter sheath, respectively.

#189970 - $15.00 USD Received 6 May 2013; revised 24 Jul 2013; accepted 30 Jul 2013; published 30 Aug 2013

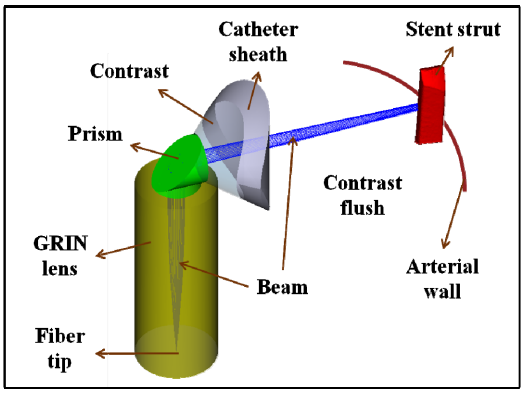

Fig. 3. Geometry of IVOCT catheter model and stent strut

To simulate the reflection and scattering of light from a stent strut, the stereolithography (STL) object file obtained from Micro-CT imaging was imported into the IVOCT catheter model (Fig. 3). Arterial tissue was added adjacent to the strut and Lambertian surface scattering was assumed to include roughness of the contrast-vessel interface. Flush fluid in the lumen is weakly scattering with a scattering coefficient of $\mu_s = 0.2$ mm^{-1}, corresponding to a residual 0.4% blood concentration [12]. Specular reflection was assumed for the strut and light backscattered from the strut was collected into a 10 μm diameter pupil and coupled back into the catheter. Rotation of the IVOCT catheter and angular sweep of the light beam over the stent strut was simulated at different eccentric positions corresponding to a 3 mm diameter vessel lumen. To examine the effect of beam size, distance between the catheter and strut was varied along the diameter of the vessel perpendicular to the flat side of the strut, corresponding to catheter offsets from the vessel center of $r_c = -0.50$, 0.0, 0.50 and 1.00 mm, Fig. 4(a). The simulation was also completed for the case when the catheter was shifted from the vessel center along the diameter parallel to the flat side of the strut, at catheter offsets from the vessel center of $r_c = 0.0$, 0.30, 0.60 and 0.95 mm, changing the location of incident beam on the strut, Fig. 4(b).

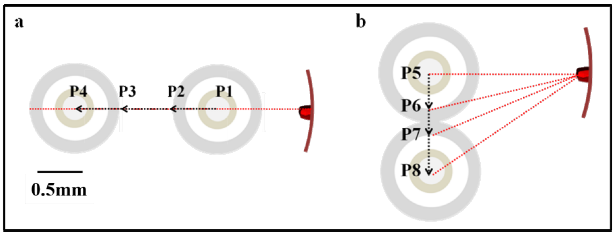

Fig. 4. Stent strut orientation with respect to IVOCT catheter: **a)** Catheter positions along the diameter of the vessel perpendicular to the flat side of the strut, $r_c = -0.50$ (P1), 0.00 (P2), 0.50 (P3) and 1.00 mm (P4), **b)** Catheter positions along a diameter parallel to the flat side of the strut, $r_c = 0$ (P5), 0.30 (P6), 0.60 (P7) and 0.95 mm (P8).

At each of the eight eccentric positions, fiber in the IVOCT catheter was rotated over the strut with an angular range of 20 degrees in 0.5 degree steps and 100,000 rays were traced at each angular position. Measured parameters included: coordinate locations on the stent strut of returned rays; intensity and direction-of-cosines of the rays returning to the fiber tip and optical pathlength (*OPL*) of light returning to the catheter. To simulate rotation of the catheter, position and orientation of strut with respect to catheter were changed for each angular step and a non-sequential ray trace was completed. Ray data was imported to MATLAB R2013a (MathWorks, Natick, Massachusetts) for further analysis. Ray trace analysis as employed in Zemax describes the propagation of light and does not take into

#189970 - $15.00 USD Received 6 May 2013; revised 24 Jul 2013; accepted 30 Jul 2013; published 30 Aug 2013

account the behavior of wave fronts. Coupling coefficient into SMF-28 fiber was determined by computing the amplitude of the overlap integral between the plane waves representing the returned rays and the fiber mode. The resulting intensity was then convolved with the source longitudinal point-spread function corresponding to a full-width half maximum Gaussian spectral width of 50nm. Data was presented in logarithmic scale (dBm) vs. depth in microns. A polar-to-cartesian conversion was performed on the A-scans to obtain simulated IVOCT images.

3. Results

When shifting the catheter from positions P1 to P4, Fig. 4(a), as the distance between the catheter and the strut increases, the IVOCT geometric beam size (i.e., without diffraction) incident on the strut first becomes smaller, from 22 × 22 μm^2 at P1 to 8 × 8 μm^2 at P2 - near the focal point and then increases to 37 × 37 μm^2 at P3 and 66 × 66 μm^2 at the most distant catheter position (P4). The measured size of the strut in the IVOCT image varies non-uniformly; from 135 μm (P1), to 100 μm (P2), 150 μm (P3) and 225 μm (P4) as distance between the catheter and strut is increased (Fig. 5). Considering the actual size of the strut is 90 μm, the effect of beam size introduces 60% error at r_c = –0.5 mm, 11% error at r_c = 0 mm, 67% error at r_c = 0.5 mm and 189% error at r_c = 0.5 mm. At increased distances from the beam focus, IVOCT signal amplitude decreases and apparent strut blooming (along the light direction) appears less.

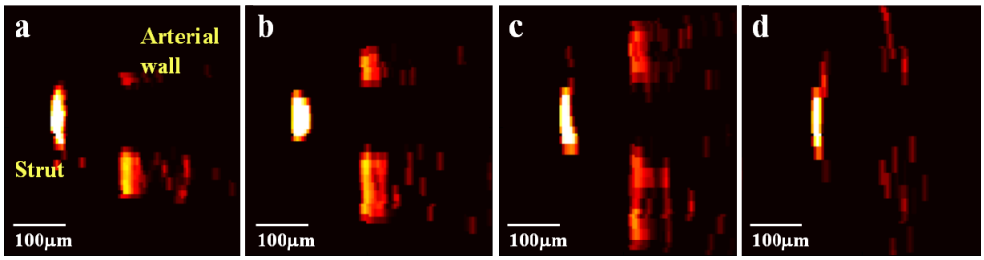

Fig. 5. Simulated IVOCT images of a CYPHER stent strut at selected offsets: **a)** *P1* (r_c = –0.5 mm), **b)** *P2* (r_c = 0 mm), **c)** *P3* (r_c = 0.5 mm), **d)** *P4* (r_c = 1 mm).

Size of the strut region reflecting light into a contrast-filled 3.1 French catheter at the four catheter eccentric positions (P5-P8) was computed. Results suggest that lateral size of the strut region reflecting light back into the IVOCT catheter can be smaller than the incident beam size. Figure 6 illustrates the stent strut orientation with respect to catheter at four different eccentric positions and the incident beam size (red) and the regions reflecting light back into the catheter (yellow) at each position. At each of the catheter offsets considered, optical pathlength (*OPL*) of light returning to the catheter over the beam angular spread is nearly constant with a maximum standard deviation of 15 μm.

#189970 - $15.00 USD Received 6 May 2013; revised 24 Jul 2013; accepted 30 Jul 2013; published 30 Aug 2013

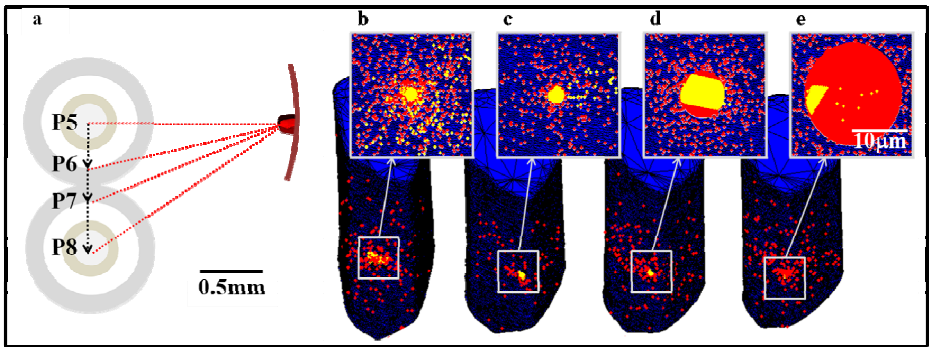

Fig. 6. **a)** Stent strut orientation with respect to IVOCT catheter at eccentric positions, incident beam (red) and regions on strut reflecting light back into the catheter (yellow) at: **b)** *P5* (r_c = 0 mm), **c)** *P6* (r_c = 0.3 mm), **d)** *P7* (r_c = 0.6 mm), **e)** *P8* (r_c = 0.95 mm).

Simulated IVOCT images of a CYPHER stent strut that is 200 μm under-deployed at catheter positions P5-P8 are shown in Fig. 7 where the apparent strut demonstrates the sunflower effect by appearing as a short line (white) directed perpendicular to the incident light beam and obliquely oriented to the luminal wall, Fig. 7(b) to 7(d).

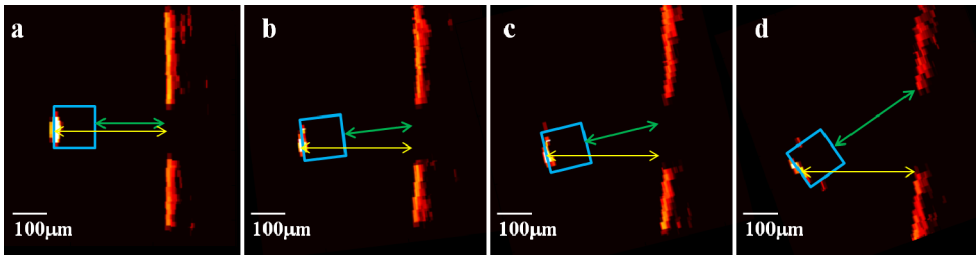

Fig. 7. Apposition measurements of a CYPHER stent strut at selected offsets: **a)** *P5* (r_c = 0 mm) **b)** *P6* (r_c = 0.3 mm) **c)** *P7* (r_c = 0.6 mm) **d)** *P8* (r_c = 0.95 mm), yellow line is drawn from center of strut blooming to the luminal wall indicating the shortest distance (approach 1), box is positioned so that edge is coincident with the leading edge of the stent and green line is drawn perpendicular to the box-edge (approach 2).

Strut apposition was measured by aforementioned two approaches. In approach 1, a line was drawn from center of the strut blooming to the luminal wall (Fig. 7; yellow lines), malapposition was determined by subtracting the known strut thickness (120 μm) from the measured distances. Measurement errors varied from 4μm at r_c = 0.0 mm to 1 μm, 4 μm and 7 μm at r_c = 0.30 mm, 0.60 mm and 0.95 mm respectively (Fig. 7). In approach 2, a 120 μm thick box was placed along the apparent IVOCT strut and a line segment from the midpoint of the opposing box-edge to luminal wall that is perpendicular to the box-edge, indicating the mal-apposed distance (Fig. 7; green lines). When the catheter is centered, the measured apposition is equivalent to the actual distance of the strut from the arterial wall. When the catheter is at eccentric positions, the measured appositions for the under-deployed strut produced artifactual errors of increased malapposition: 2 μm at r_c = 0.30 mm, 25 μm at r_c = 0.60 mm and 82 μm at r_c = 0.95 mm, Fig. 7(b) to 7(d).

4. Discussion

The two approaches to measure stent apposition give different results for catheter positions P6-P8. While approach 1 gives accurate apposition measurements for positions P6-P8, approach 2 introduces artifactual errors. Apposition measurement errors introduced when applying approach 2 at positions P6-P8 originate from misplacement of the box representing the stent strut. In these cases, placement of the box so that one box-edge is coincident with the

#189970 - $15.00 USD Received 6 May 2013; revised 24 Jul 2013; accepted 30 Jul 2013; published 30 Aug 2013

leading edge of the IVOCT strut can introduce position and orientation errors. At positions P6-P8, light reflects from a small corner or edge region of the stent strut so that strut blooming in IVOCT images is not oriented parallel to the strut edge - thereby introducing the sunflower effect. Alternatively, when the box representing the stent strut is placed correctly, Fig. 8(a), an accurate apposition measurement is obtained, Fig. 8(b). In cases when the box is not utilized, approach 1 gives consistent measures of strut apposition and is equivalent to the method first described by Ughi et al. [13] in which the line segment is perpendicular to luminal wall. When utilization of the stent strut box is desired, the box should be positioned parallel to the arterial wall, Fig. 8(b), with the corner- or edge-region touching the center of the strut blooming in the IVOCT image.

Observation of all stent struts in the IVOCT image can be used to aid estimation of strut orientation and proper placement of boxes. For example, a partially under-deployed stent where the sunflower effect is observed is shown in Fig. 8(c). To estimate malapposition, a circle is drawn tracing the circumference of the stent and boxes are placed facing the center of the stent. In this case, malapposition is determined by measuring distances from the back surface of the boxes to the luminal wall. When utilization of the stent strut box is not desired, approach 1 [13] provides accurate malapposition measurements in presence of sunflower effect.

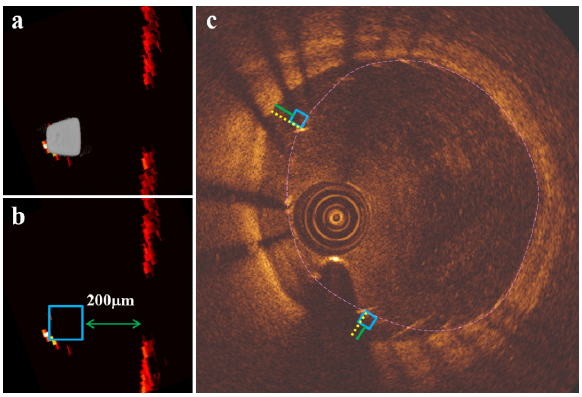

Fig. 8. **a)** Actual position of CYPHER stent strut, **b)** proper box placement provides an accurate malapposition measurement at *P8* (r_c = 0.95 mm), **c)** proper box placement based on distribution of all stent struts for accurate malapposition measurement by approach 2, yellow lines represent malapposition measurement by approach 1.

The CYPHER stent strut considered in our study represents one example of the impact caused by the stent surface curvature. For the CYPHER, strut surface curvature changes rapidly from flat areas to the edge and therefore reflecting regions where the wavefront normal matches the strut surface normal are more limited. In the case of stent struts that have a more rounded shape, this effect would be less pronounced so that reflecting regions may be larger and length of the apparent strut in IVOCT images may be longer. Results of this study suggest that IVOCT measurement of size and apposition of metallic stent struts benefits from considering the distribution of all the stent struts in an IVOCT image. Development of automated algorithms and methods to properly place the box and provide accurate estimates of stent apposition are feasible and appear warranted.

Acknowledgments

This study was supported in part by the Biomedical Engineering Advancement Fund, a VA Merit grant, Clayton Foundation for Biomedical Research, Janey and Dolph Briscoe Center for Cardiovascular Research, and the Cigarrora Endowed Professorship.